APPLICATION OF COMPUTATIONAL METHODS TO THE THERMOCHEMICAL DEGRADATION OF BIOMASS

A Thesis

Presented to the Faculty of the Graduate School

of Cornell University

in Partial Fulfillment of the Requirements for the Degree of

Master of Science

by

Kara Nicole Malhotra

August 2013

ABSTRACT

Accounting for the chemical processes in large-scale Computational Fluid Dynamic (CFD) simulations is essential to understand industrial reacting flows. The implementation of a detailed kinetic mechanism, involving a large number of chemical species and elementary reactions, can be challenging and may require unrealistic computational resources. In addition, the level of detail provided by these comprehensive mechanisms might be excessive, especially when accounting for the modeling uncertainties involved in the simulations. Proposed below is a systematic strategy to reduce a detailed kinetic model into a global model that will: (i) contain many fewer reaction steps, (ii) use lumped variables that combine species of similar chemical nature, and (iii) maintain the predictive capabilities of the detailed mechanism for the quantities of interest. The approach is demonstrated here in the context of biomass gasification. Partially stirred reactor (PaSR) models are used in conjunction with a detailed chemical kinetic mechanism to generate a database of gas phase detailed compositions likely to occur in an actual reactor. From the analysis of this database, representative lumped species are identified, for which effective elemental formula, molecular weight, and thermodynamical properties are determined. An appropriate set of global reactions describing the evolution of these lumped species is then proposed, whose rate coefficients in Arrhenius format are fitted to match production rates formed from the sampled detailed compositions and detailed kinetic scheme. Validation is performed by comparing the PaSR dynamics predicted using the detailed and global models.

BIOGRAPHICAL SKETCH

Kara Malhotra earned her Bachelor of Science degree in Chemical Engineering from Cornell University in 2011. She directly entered into a Master's degree program in Mechanical Engineering at Cornell the following year, and then spent the second year of her Master's program conducting research at the National Renewable Energy Labs in Golden, CO. At NREL she had the opportunity to get involved in experimental work, contribute to other groups conducting high level techno-economic studies, and consult an industrial company pursuing gasification. Her work has been presented at the ACS National Meeting in 2012 as well as the 2013 National Combustion Meeting. Kara's thesis, entitled "Application of Computational Methods to the Thermochemical Degradation of Biomass" was supervised by Dr. Perrine Pepiot and Dr. Elizabeth Fisher.

I would like to dedicate my thesis to my Mom and Dad, Mary and Shan Malhotra, my sister's Laura and Mia Malhotra, my brother Mark Malhotra, my grandparents, Kamini and Sudarshan Malhotra and Bob and Elene Chamberlain. These people have offered me infinite love and support throughout my life and always inspired me to pursue my passions, wherever they may take me.

ACKNOWLEDGEMENTS

I would like to acknowledge first and for most my advisor, Dr. Pepiot. She has guided my research for the last two years, and had the patience and diligence to train me as I entered a new field. She has granted me the unique opportunity to experience collaboration within a National lab, while still helping me maintain momentum and progress in our own research.

I would also like to acknowledge Professor Fisher, who initially sparked my interest in energy and fuels. Her involvement and passion for research in biomass and sustainability has always been inspirational to me, and I thank her for her continued support during my time at Cornell.

I also would like to acknowledge the scientists at NREL that I worked closely with including Peter Ciesielski, Bryon Donohoe, Anna Trendewicz, Abhijit Dutta, Mark Nimlos, and Ray Grout. They helped me get involved in interesting and impacting projects at NREL, that I am very appreciative I had the chance to contribute to.

TABLE OF CONTENTS

LIST OF TABLES

LIST OF FIGURES

CHAPTER 1

INTRODUCTION

Thermal degradation of biomass is emerging as a promising option for producing liquid transportation fuels from renewable sources, but further research is needed to identify optimal process conditions that will allow liquid fuel production from biomass to become economically viable. Combined with empirical expertise, computational tools can be used to better understand how reactor conditions, pretreatment, or biomass characteristics can be chosen to either maximize the production of bio-oils during pyrolysis, or limit undesirable tar formation in synthesis gas production from gasification. Experiments show that key properties of the conversion process, for instance, undesirable Polycyclic Aromatic Hydrocarbon in gasification, are determined by subtle aspects of the chemical processes and their interactions with the surrounding multiphase flow environment [7]. Yet, those processes and interactions are seldom considered in adequate detail in most modeling efforts due to their inherent complexity. In this context, we propose a systematic strategy to generate, from knowledge obtained using detailed kinetic chemical mechanisms, extremely compact schemes suitable for use in CFD simulation of biomass thermochemical conversion reactor.

Previous studies have hypothesized a general chemical mechanism for gasification [10]. During heating of biomass at low temperatures, primary volatiles are released from the cellulose, hemicellulose, and lignin solid. Heating of the primary volatiles will induce thermal cracking to small hydrocarbon and radical species. Finally at higher temperatures during gasification, the small hydrocarbons will polymerize into high molecular weight Polycyclic Aromatic Hydro-

carbon molecules. This general mechanism is depicted in Fig 1.1.

There are a variety of global kinetic models that have been proposed for biomass pyrolysis and gasification as reviewed by DiBlasi and Prakash [5, 16]. In general these models propose a mechanism (on the order of five reactions) and fit the mechanism to various forms of empirical data. The models discussed can be classified into: multicomponent devolatilization models that only predict solid mass loss (often contains three reactions for cellulose, hemicellulose, lignin), single and multicomponent models for primary pyrolysis that predict solid, tar, and gas yields, and models that further incorporate secondary gas reactions. For example, one of the most sophisticated of these global models considers parallel reactions for cellulose, hemicellulose, and lignin volatilization as well as secondary gas phase reaction of tar vapors to gas. The proposed mechanism is fit to TGA data to predict final yields of tar, gas and char [12]. While this model and the others discussed by Prakash and DiBlasi may artificially predict the product distribution, they ignore inherent chemical mechanisms such as thermal cracking and polymerization.

Additionally, most of the available global mechanisms lack information about the volatile species produced: they cannot predict the amount of PAH components produced (which add cost to processing the synthesis gas) or the relative amounts of H_2 and CO produced (which affects the process conditions for producing fuel from synthesis gas). Those proposed mechanisms that have attempted to describe detailed species are heavily parameterized [17, 22]. Therefore, the available global models are not suitable because they: 1) do not provide detail about species of interest and 2) ignore subtleties of the chemistry such as polymerization that are believed to be key chemical features with the potential

to be optimized for industrial performance.

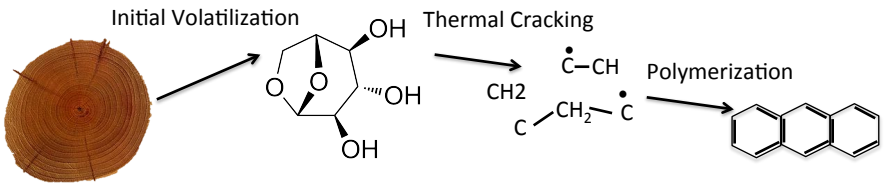

Figure 1.1: General hypothesized mechanism for biomass thermal degradation.

Recent progress in the understanding of the chemical reaction pathways occurring during biomass thermochemical conversion have led to the development of semi-detailed kinetic mechanisms combining a large number of elementary reaction steps. Ranzi *et al.* [6, 2, 3, 18] proposed a fairly detailed description of the biomass devolatilization chemistry involving 15 solid species, and coupled this solid-gas reaction set to a gas-phase kinetic scheme for hydrocarbon oxidation. A similar approach was followed by Pepiot *et al.* [15], with a focus on PAH formation during biomass gasification at relatively high temperature.

Such mechanisms can involve hundreds of molecular species and thousands of reactions steps, which prohibits their direct use in CFD. However, assuming that they provide an accurate description of the actual chemical kinetics in the conversion process of interest, they can be used in lieu of experimental data in the development of global models. While a large number of efficient chemistry reduction techniques have been developed of this purpose in the context of hydrocarbon combustion, these techniques are ill-suited for biomass applications due to the nature of the multiphase flows involved, and would not provide the high degree of reduction we are looking for. Here, we propose to combine an analysis of the reaction pathways described in the detailed model with a mathematical lumping approach and simple rate fitting procedure to automatically

generate a set of global reactions able to reproduce the relevant chemical features of the detailed model.

The methodology to systematically derive a global model from a detailed mechanism is first described in Chapter 2. Using biomass gasification as an example, illustrations of the various steps and validation of the method are provided in Chapter 3.

CHAPTER 2

METHODOLOGY

2.1 Overview

To provide a clear overview of the proposed strategy for global model development, it is worthwhile to start by introducing some relevant definitions and notations. The set of detailed species appearing in a given chemical kinetic mechanism is denoted as $\mathbf{\Phi}^D$, of cardinality n_D. These species usually correspond to actual molecular compounds. The elemental composition of detailed species i, the number of atoms of carbon, hydrogen, oxygen and nitrogen in a molecule of species i, is referred to as N_i^D. We will designate the elements of this set as $\phi^D_{i,i=1..n_D}$. The set of elementary reactions included in the detailed model is denoted as $\mathcal{R}^D$, of cardinality $n_{\mathcal{R}^D}$. Any reaction in $\mathcal{R}^D$ only involves species in $\mathbf{\Phi}^D$.

In a similar way, a global kinetic model is characterized by its set of global species $\mathbf{\Phi}^G$, of cardinality $n_G < n_D$. These species will be designated by $\phi^G_{i,i=1..n_G}$. The set of elementary reactions included in the global model is denoted as $\mathcal{R}^G$, of cardinality $n_{\mathcal{R}^G}$. Any reaction in $\mathcal{R}^G$ only involves species in $\mathbf{\Phi}^G$. We impose that each ϕ_i^G be explicitly defined as a composite of one or more detailed species, and therefore may not be associated with any single molecular compound. In this case, we can further define for each global species i the subset of detailed species involved in the definition of ϕ_i^G: $\mathbf{\Phi}^{D,i}$. If we assume that the detailed

species can contribute to one single global species only, we can write:

$$\begin{aligned} &\left\{\mathbf{\Phi}^{D,i}, i = 1, n_G\right\} = \mathbf{\Phi}^G \\ &\cap \left\{\mathbf{\Phi}^{D,i}, \mathbf{\Phi}^{D,j}\right\} = \emptyset \text{ for any pair } \{i \neq j\} \end{aligned} \tag{2.1}$$

Let the n_D-vector C^D denote the composition of the gas-phase mixture in terms of the detailed species $\phi^D_{i,i=1..n_D}$, and the n_G-vector C^G the composition in terms of the global species $\phi^G_{i,i=1..n_G}$. We also introduce the mapping of quantities defined for detailed species, Z^D, to the model species space as:

$$\widehat{Z^G} = \mathbf{B} Z^D \,, \tag{2.2}$$

where $\mathbf{B}$ is a $n_G \times n_D$ matrix defined as $B_{i,j} = 1$ if $\phi^D_j \in \mathbf{\Phi}^{D,i}$, 0 otherwise.

Finally, we will denote by $\mathcal{D}$ an ensemble of detailed compositions $C^D_{i,i=1..n_\mathcal{D}}$, where $n_\mathcal{D}$ is the cardinality of $\mathcal{D}$, and their corresponding production rates, $\left(dC^D/dt\right)_{i,i=1..n_\mathcal{D}}$.

The strategy proposed here for the development of global kinetic schemes is based on the simple observation that if the ensemble $\mathcal{D}$ contains an adequate sampling of compositions likely to be encountered in the application of interest, the best global model would be one for which, for each sample composition in $\mathcal{D}$:

$$\begin{aligned} C^G = \widehat{C^G} &= \mathbf{B} C^D \,, \\ \left(\frac{dC}{dt}\right)^G = \left(\widehat{\frac{dC}{dt}}\right)^G &= \mathbf{B}\left(\frac{dC}{dt}\right)^D \end{aligned} \tag{2.3}$$

that is, the concentrations and production rates for the global species as provided by the set of global reactions are exactly equal to the concentrations and production rates for the global species obtained by mapping of the detailed production rates. This exact linear lumping situation being virtually impossible to

obtain in practice, the ability of a global model to reproduce the prediction of the detailed mechanism is a direct function of how well Eq. 2.3 is satisfied on average.

Our approach to construct a global model that closely satisfies Eq. 2.3 consists in the following steps:

1. Create a database of a large number of compositions likely to be observed in the reactor configuration of interest. This step will be done using the computationally cheap Partially Stirred Reactor (PaSR) model;
2. Identify the set $\mathbf{\Phi}^G$ of global species and corresponding mapping matrix $\mathbf{B}$;
3. Determine thermochemical properties for the global species, including elemental composition, molar mass, heat capacity, and enthalpy;
4. Identify a set of balanced global reactions involving species $\phi^G_{i,i=1..n_G}$ that provide appropriate consumption and reactions pathways for all global species;
5. Determine rate coefficients in Arrhenius format (to maintain compatibility with existing chemistry and CFD software) for each global reactions.

Each of these steps are described in more detailed in the following subsections, note that except for the definition of the global species set and how they involve the detailed species, which may require some chemistry knowledge, all steps are systematic and automatic, require *very limited* user input, and *do not involve tuning or non-linear optimization procedure*.

2.2 Sample compositions database

The first step in our global mechanism development is to build a set of compositions representative of the gas compositions relevant to the reactor conditions of interest. A PaSR model is used for this purpose, the details of which are provided in Section 3.1 for biomass gasification. An entry n in the database consists of the concentration vector for the detailed species, C_n^D, the corresponding production rate vector $dC/dt|_n$ as provided by the detailed kinetic mechanism, and the temperature T_n.

2.3 Definition and thermochemical properties of global species

We assume that the global species $\mathbf{\Phi}^G$ and their definition in terms of the detailed species, $\mathbf{\Phi}^D$, the species sets $\mathbf{\Phi}^{D,i}, i = 1, n_G$ are known. This uniquely determines the mapping matrix $\mathbf{B}$. The relative molar contribution of any detailed species ϕ_j^D to a global species ϕ_i^G is defined for a given composition vector C_n^D as:

$$P_{j,n}^i = \frac{C_{j,n}^D}{\sum_{i=1}^{n_D} B_{i,j} C_{j,n}^D} = \frac{C_{i,n}^D}{\widehat{C}_{i,n}^G} \tag{2.4}$$

Note that in the equation above and in the following, Einstein summation is assumed. In general, this relative contribution is different for each sample composition. Therefore, we define the average global species composition as:

$$\left\langle P_j^i \right\rangle = \frac{1}{n_{\mathcal{D}}} \sum_{n=1,n_{\mathcal{D}}} P_{j,n}^i \,. \tag{2.5}$$

From this, we define the elemental composition of global species j as:

$$N_j^G = \left\langle P_j^i \right\rangle N_i^D \tag{2.6}$$

and the molar mass of global species j as

$$W_j = N_j^G \cdot W^a \,, \tag{2.7}$$

where the W^a vector contains the atomic mass of the involved atoms: carbon, hydrogen, oxygen, and nitrogen.

For each sample n in the database, the molar heat capacity $C_{p,i}^n$ and molar enthalpy H_i^n of a global species i are evaluated from those of the detailed species and the contribution vector $\mathbf{P}_i$ according to:

$$C_{p,i}^n(T_n) = \mathbf{P}_i \cdot C_{p,j}^n(T_n) H_i^n(T_n) = \mathbf{P}_i \cdot H_j^n(T_n) \tag{2.8}$$

The mean heat capacity and enthalpy conditioned on the temperature, $\left\langle C_{p,i}|T \right\rangle$ and $\langle H_i|T \rangle$, are then evaluated. The molar heat capacity and enthalpy of each global species are finally expressed as:

$$\frac{C_{p,i}}{R} = a_1 + a_2 T + a_3 T^2 \tag{2.9}$$

$$\frac{H_i^0}{RT} = a_1 + \frac{a_2}{2} T + \frac{a_3}{3} T^2 + \frac{a_4}{T} \tag{2.10}$$

where the coefficients a_1, a_2, a_3, and a_4 are obtained by fitting the conditional means to a quadratic polynomial to conform to NASA standard format for thermodynamic data (additional coefficients in NASA format are simply set to zero).

2.4 Global reaction pathways

A major challenge when developing multi-steps global models is to identify appropriate reaction pathways between global species. This is further complicated by the fact that those pathways have to satisfy element conservation. Here, we

proceed in two successive steps. The first one analyzes the detailed reaction network to provide an appropriate set of global reactions, the second adjusts the stoichiometric coefficients to satisfy element conservation. Details are provided for both steps in the following subsections.

2.4.1 Initial global reaction network

The detailed compositions database, coupled with the detailed kinetic mechanism is used to quantify the coupling between global species (whose concentrations are estimated here from the detailed compositions and mapping equation (2.2)), and provide information on the most appropriate production and consumption route of each global species. We apply the following rules to automatically generate a consistent set of global reactions:

1. Based on the ratio between species production and consumption rates, separate the set of global species into a products set, which includes species having negligible consumption rates, an exchange set, which includes species with large, but nearly equal production and consumption rates, and a reactants set (all other species). One consumption reaction will be written for each species in the reactants set, while species in the products set will only appear as products in the global reactions. Species in the exchange set are expected to contribute indifferently as reactant or product in most reactions.
2. The consumption and production of global species i from a detailed reac-

tion j are defined respectively as:

$$C_{ij} = \max\left\{0, -B_{ik}\nu_{kj}^{D}Q_j\right\} \tag{2.11}$$

$$\mathcal{P}_{ij} = \max\left\{0, B_{ik}\nu_{kj}^{D}Q_j\right\} \tag{2.12}$$

where B is the mapping matrix, ν_{ij}^{D} is the stoichiometric coefficient of detailed species i in detailed reaction j, and Q_j is the reaction rate of detailed reaction j. C and $\mathcal{P}$ are therefore matrices of size $n_G \times n_{\mathcal{R}^D}$. We further define the corresponding normalized matrices δ^C and $\delta^{\mathcal{P}}$ as:

$$\delta_{ij}^{C} = 1 \text{ if } C_{ij} > 0, \quad 0 \text{ otherwise, and} \tag{2.13}$$

$$\delta_{ij}^{\mathcal{P}} = 1 \text{ if } \mathcal{P}_{ij} > 0, \quad 0 \text{ otherwise.} \tag{2.14}$$

The relative consumption of a global species i in the intermediates species set from detailed reactions producing global species j is then:

$$\eta_{ij}^{P} = \frac{C_{ik}\delta_{jk}^{\mathcal{P}}}{\sum_{k=1}^{n_G} C_{ik}}, \tag{2.15}$$

which can be interpreted as the product distribution from the consumption of global species i. A global species j is included as a product in the consumption reaction of global species i if

$$\eta_{ij}^{P} > \varepsilon, \tag{2.16}$$

with ε a small user-defined coefficient, usually of order 10^{-3}. The corresponding stoichiometric coefficient is initially set to η_{ij}^{P}.

3. In a similar way, we can compute the relative consumption of global species i from detailed reactions also consuming global species j:

$$\eta_{ij}^{R} = \frac{C_{ik}\delta_{jk}^{C}}{\sum_{k=1}^{n_G} C_{ik}}, \tag{2.17}$$

which is used to identify the most likely reactant partner for species i. The stoichiometric coefficient of this second reactant j is initially based on the value of η_{ij}^R.

Note that at this stage, no guarantee exists that the constructed global reactions satisfy element conservation.

2.4.2 Reaction balance

To ensure element balance, and therefore, mass conservation in the simulation, the initial values of the stoichiometric coefficients chosen in Section 2.4.1 have to be adjusted to account for the global species properties determined in Section 2.3. Linear programming is used to find, for each global reaction r, the smallest increment in the stoichiometric vector $\mathcal{S}^r$, containing the stoichiometric coefficients of each species, reactant or product, involved in reaction r, necessary to obtain element balance across the reaction. The stoichiometric coefficient of the main reactant, for which the consumption reaction was written, is imposed equal to unity. Minimum bounds are imposed on the stoichiometric coefficient increment to ensure that all species are retained in the reaction after linear programming.

2.5 Global reactions rate coefficients

This subsection describes how rate coefficients in Arrhenius format are determined for each of the global reaction steps. In the current implementation, the

standard law of mass action is used to compute reaction rates to ensure compatibility with chemistry and CFD software. However, it is important to note that since global steps are not elementary reactions, their assigned rates do not carry the same chemical meaning as elementary steps and could be taken to be any general function of temperature and species composition. The steps followed to determine a set of rate coefficients for each global reactions are outlined below:

1. All compositions included in the sample database $\mathcal{D}$ are binned based on their temperature. The number and temperature range of each bin is determined so that it contains a large enough number of composition samples. We denote by n_B the number of bins. The median temperature of bin b is T_b.

2. For each bin b, we want to find the reaction coefficient vector k_b of size $n_{\mathcal{R}^G}$ that minimizes over all sample compositions n included in bin b, the distance between the global species production rates as evaluated from the detailed composition and kinetic model:

$$\left.\widehat{\frac{dC}{dt}}\right|_n = B \left.\frac{dC^D}{dt}\right|_n , \tag{2.18}$$

and those evaluated according to the global reaction steps defined above:

$$\left.\frac{dC^G}{dt}\right|_n = \sum_{j=1}^{n_{\mathcal{R}^G}} \nu_{ij}^G Q_j^G , \tag{2.19}$$

with

$$Q_j^G = k_j(T_b) \prod_{\text{reactants } n} \left(C_n^G\right)^{\nu_{nj}} . \tag{2.20}$$

For each temperature bin b, this leads to an over-determined system of equations for the unknowns $k_b(T_b)$, which is solved using a weighted least-square approach.

3. Finally, the resulting $k_b(T_b), b = 1, n_B$ are fitted to a 2-parameter Arrhenius form to yield:

$$k_j(T) = A_j e^{-\frac{E_j}{RT}}, j = 1..n_{RG} \tag{2.21}$$

CHAPTER 3

APPLICATION TO BIOMASS GASIFICATION CHEMISTRY

The methodology outlined above is applied to the development of a global mechanism for biomass gasification, starting from the semi-detailed mechanism described in Pepiot *et al.* [15]. Illustrations for the main steps of the algorithm are provided below.

3.1 Sample compositions database for biomass gasification at high temperature

A partially stirred reactor (PaSR) model tailored for biomass devolatilization and secondary gas phase chemistry is used to assemble a database of gas compositions likely to be observed in a realistic conversion reactor. A PaSR is a statistical reactor in which notional particles carrying chemical compositions evolve through reactions (according to a specified chemical mechanism), and mixing (here, a pair-wise mixing model is employed). Computationally cheap to run, it allows to conveniently handle the non-trivial gas phase source terms arising from biomass devolatilization. The two inflow streams are pure nitrogen at high temperature, and appropriate biomass devolatilization products as determined from Ranzi et al. [18] solid biomass chemistry model. The PaSR parameters used in this example are shown in Table 3.1. Once the PaSR reaches steady-state, the compositions of the particles are collected over several residence times. The database consists of 5,000 distinct compositions, corresponding production rate vectors, and temperature.

Parameter	Value
Number of particles in PaSR	100
Gas residence time	1s
Mixing time	0.1 s
Biomass particle heating rate	1000K/s
Temperature of raw biomass	300K
Temperature of pure nitrogen stream	1000K
Normalized mass flow rates of nitrogen and biomass streams	0.6, 0.4

Table 3.1: PaSR parameters used to build the sample compositions database for biomass gasification.

3.2 Global species definition and thermochemical properties

The 187 detailed species contained in the detailed chemical model are grouped into global species according to the following *ad hoc* approach. Species of particular interest and/or high concentration, such as methane and carbon monoxide, are kept as individual species. Three groups are formed that represent the initial biomass volatile products. Then, species containing linear chains of carbon are grouped according to the number of carbon atoms they contain: C_1-C_2, C_3-C_4, and C_5-C_6-C_7. Then those molecular species in C_3-C_4 and C_5-C_6-C_7 that contain oxygen are further separated into groups C_3-C_4O and C_5-C_6-C_7O. Finally, ring species are categorized into two groups: the first one contains molecules with one aromatic ring, and the second contains the heaviest species with two or more aromatic rings. These global species are listed in Table 3.2, and their mean concentrations and production rates as function of the temperature, computed from the composition database and the mapping matrix B, are shown in Fig. 3.1

The elemental composition and molecular weight of each global species are determined using the method described in Section 2.3, and the results are shown in Table 3.2. Heat capacity and enthalpy for each global species are determined

Global Species	Formula	W (kg/mol)
N_2	N_2	0.028
CO_2	CO_2	0.044
CO	CO	0.028
CH_4	CH_4	0.016
H_2O	H_2O	0.018
H_2	H_2	0.002
BV_1	$C_{2.271}H_{4.256}O_{1.728}$	0.0592
BV_2	$C_{5.936}H_{6.126}O_{3.063}$	0.1265
BV_3	$C_{7.059}H_{10.366}O_{4.673}$	0.1700
C_{1-2}	$C_{1.296}H_{3.376}O_{0.945}$	0.0341
C_{3-4}	$C_{2.207}H_{5.855}$	0.0324
$C_{3-4}O$	$C_{3.1124}H_{4.709}O_{2.510}$	0.0823
C_{5-7}	$C_{5.914}H_{5.995}$	0.0771
$C_{5-7}O$	$C_{5.170}H_{4.679}O_{2.339}$	0.1042
R_1	$C_{6.637}H_{7.273}O_{1.529}$	0.1115
R_2	$C_{10.000}H_{8.000}$	0.1282

Table 3.2: List of global species used in the global mechanism, and corresponding elemental composition and molar mass.

from their detailed species counterparts according to Section 2.3. Very good fits are observed in general over the range of temperatures of interest, with the largest scatter obtained for those global species involving the largest number of detailed species. Examples of such fits for three global species are shown in Fig 3.2.

3.3 Development of a set of global reactions and corresponding rate coefficients

The relative consumption matrices η^P and η^R defined in Section 2.4.1 are generated from the database compositions, and are shown in Fig. 3.3. From the analysis of these matrices, a set of global reactions is determined, each one de-

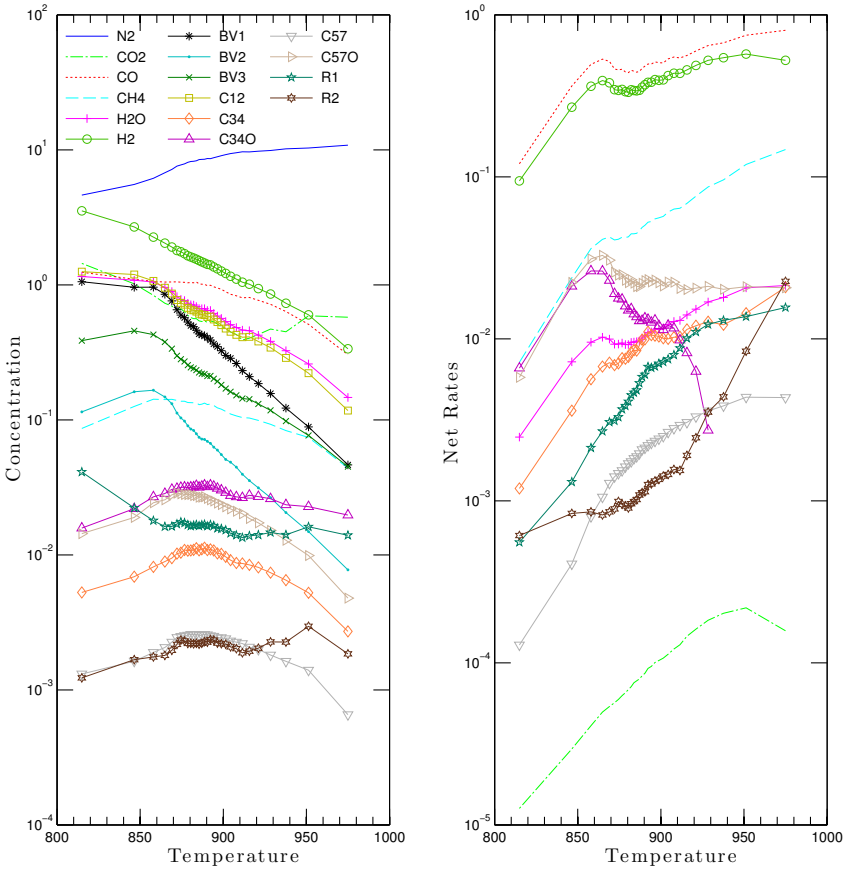

Figure 3.1: Average concentration (left) and net rate (right) as a function of temperature: data generated from detailed kinetic mechanism and processed into lumped species

scribing the consumption of global species identified as reactants, , BV_1, BV_2, BV_3, C_{34}, $C_{34}O$, C_{57}, $C_{57}O$, R_1, and R_2. Linear programming is employed to ensure element balance for each reaction. The final set of global reactions is listed in Fig. 3.3.

The rates for each global reaction were determined from a weighted least-square to match as well as possible the production rates provided by the detailed composition database, according to the procedure outlined in Section 2.5. The resulting reaction rates are shown in Fig. 3.4, along with the best 2-

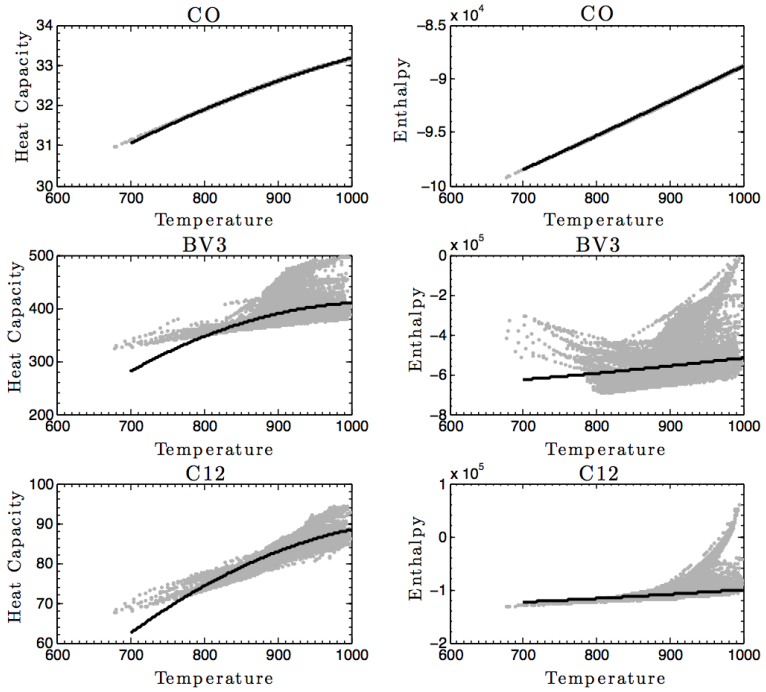

Figure 3.2: Quadratic fitting of heat capacity and cubic fitting of the enthalpy as a function of temperature for three selected global species.

parameter Arrhenius fit. Little scatter is observed, indicating that the global reactions are appropriate to describe the evolution of the specified global species. Such good agreement is facilitated by the relatively slow chemistry involved in the gas phase. Comparison between the mean production rates derived from the database and those obtained from the global reaction scheme is shown in Fig 3.5. While the agreement is far from perfect, trends are accurately captured for all global species.

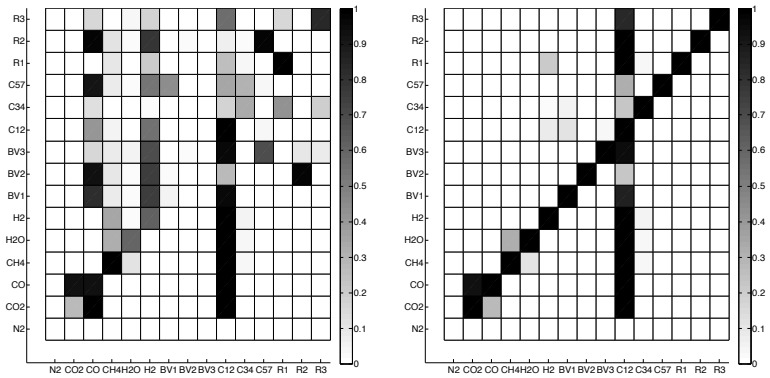

Figure 3.3: Relative production (left) and consumption (right) matrices used to systematically identify appropriate global chemical pathways. Dark color indicates high level of coupling between the two corresponding global species.

Table 3.3: Final lumped mechanism and associated rate constants

Reaction	A [m^3-mol-kg]	E [kJ/mol]
$BV_1 + 0.3388C_{12} \xrightarrow{k1} 0.9615CO + 0.04529CH_4 + 0.0079H_2O + 0.3775H_2$ $+1.142C_{12} + 0.1012C_{34}$	4.03299×10^{14}	251.449
$BV_2 + 0.0145C_{12} \xrightarrow{k2} 0.5899CO + 0.0497CH_4 + 0.0132H_2O + 0.3769H_2$ $+0.0112BV_1 + 0.1365C_{12} + 0.0071C_{34} + 0.0165C_{34}O + 0.9759C_{57}O$	1.88994×10^{10}	169.769
$BV_3 + 0.0949C_{12} \xrightarrow{k3} 0.3446CO + 0.0458CH_4 + 0.0283H_2O + 0.3462H_2 + 0.1973BV_1$ $+0.4799C_{12} + 0.0064C_{34} + 1.2557C_{34}O + 0.0479C_{57}O + 0.0441R_1 + 0.0535R_2$	1.68470×10^{6}	117.037
$C_{34} + 0.3660C_{12} \xrightarrow{k4} 0.0688CO + 0.4761CH_4 + 0.0008H_2O + 1.3853H_2 + 0.0043BV_1$ $+0.0870C_{12} + 0.0073C_{34}O + 0.2163C_{57} + 0.0058C_{57}O + 0.1011R_1 + 0.0010R_2$	1.5875×10^{7}	106.231
$C_{34}O + 0.0189C_{12} \xrightarrow{k5} 1.2796CO + 0.0400CH_4 + 0.1231H_2O + 0.2674H_2$ $+0.5533BV_1 + 0.1785C_{12} + 0.1492C_{34}$	1.7074×10^{2}	28.961
$C_{57} + 0.1319C_{12} \xrightarrow{k6} 0.0481CH_4 + 0.0003H_2O + 0.1031H_2 + 0.1256C_{12}$ $+0.2228C_{34} + 0.0003C_{57}O + 0.0032R_1 + 0.5359R_2$	1.14230×10^{10}	157.296
$C_{57}O + 1.744C_{12} \xrightarrow{k6} 0.4875CO + 0.0558CH_4 + 0.0107H_2O + 0.3969H_2 + 0.7283BV_2$ $+0.03772C_{12} + 0.4515C_{34} + 0.4875C_{34}O$	9.06770×10^{8}	136.516
$R_1 + 0.0031C_{12} \xrightarrow{k7} 0.6387CO + 0.0002CH_4 + 0.0199H_2O + 0.0900H_2$ $+0.9236C_{12} + 0.0790C_{57} + 0.4336R_2$	2.8760×10^{1}	390.39
$R_2 + 3.9682C_{12} \xrightarrow{k8} 0.0888H_2O + 2.0495H_2 + 0.2692C_{12} + 2.2292R_1$	1.33155×10^{3}	443.85

3.4 Validation of the global model in a PaSR

The final global mechanism is used in PaSR to obtain the evolution of the global species mass fraction as function of time as predicted by the global model. Re-

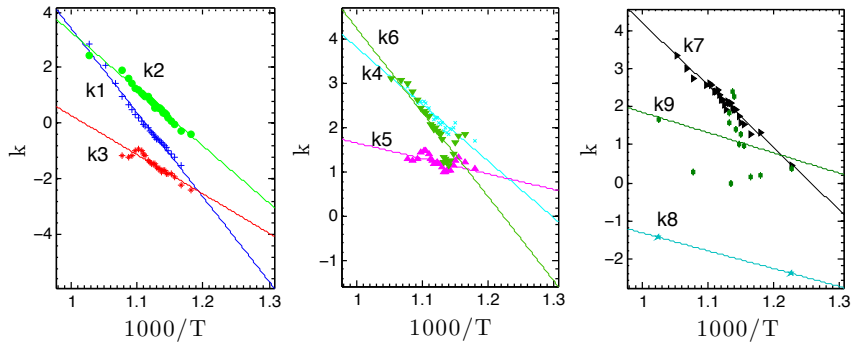

Figure 3.4: Fitting of the rate constants derived for the global model into an Arrhenius type form

sults are shown in Fig. A.1. A very good agreement is obtained for most species, with some discrepancy observed for the ring species, demonstrating that the derived global mechanism, with 9 reaction steps involving 15 global species only, is able to reproduce the dynamics of the detailed 187-species, 2200-reaction model accurately.

Next we wished to see if the same procedure can be utilized for a more general case. This time, many PaSR reactors were run ranging in temperature from 950 K to 1150 K. The same procedure was employed to get a global model for this compositional database. Then the global mechanism was tested in multiple reactors ranging again from 950K to 1150 K. In each case, the equilibrium mass fraction data was acquired. The mean mass fraction as a function of PaSR temperature obtained from applying the global and detailed model are shown in Fig. A.1. Considering the large range of compositions and temperatures that compose the database, most species are in quite good agreement, suggesting that this method will be applicable in a more general case in the future.

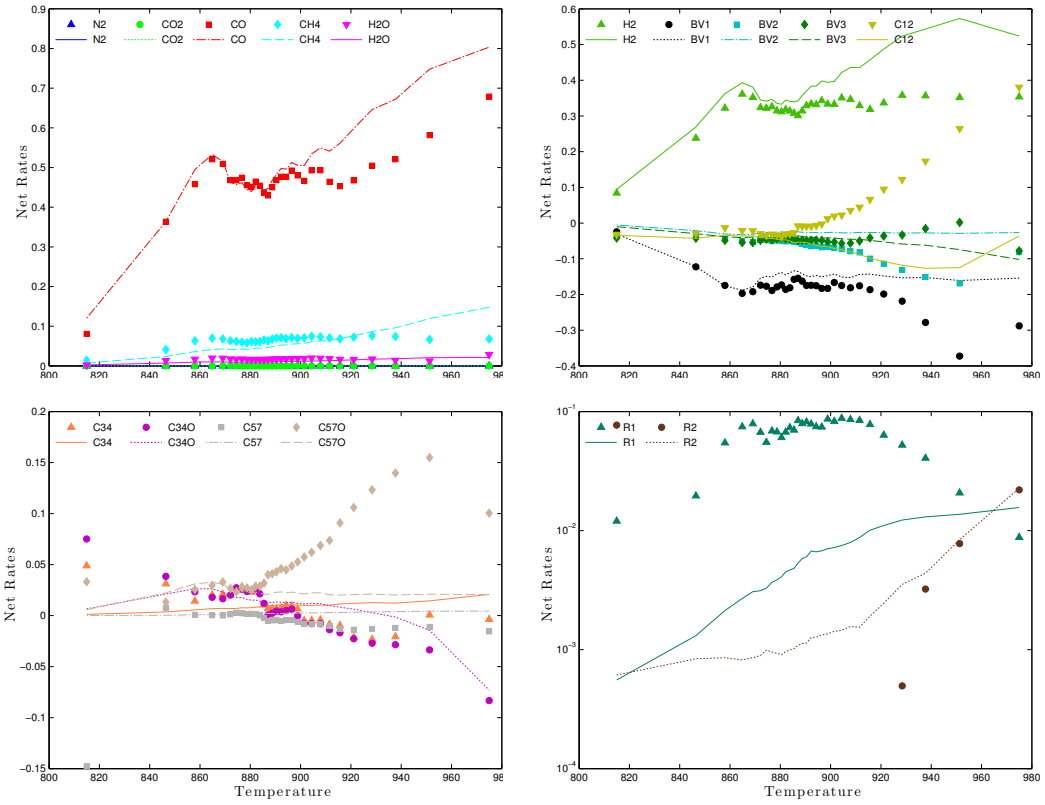

Figure 3.5: Average net rate (**mol**/**m**^{3}**sec**) of lumped species as a function of temperature (K) : global mechanism (dots) fitted to the detailed database (lines)

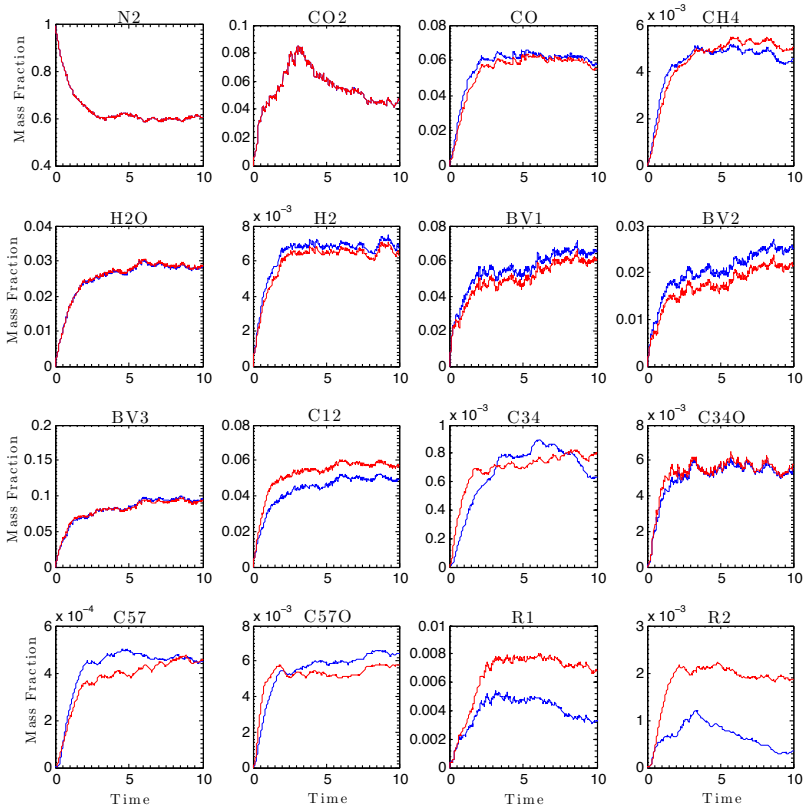

Figure 3.6: Evolution of species mass fractions in a PaSR reactor model for biomass gasification: Comparison between detailed model prediction (blue line) and global model predictions (red lines).

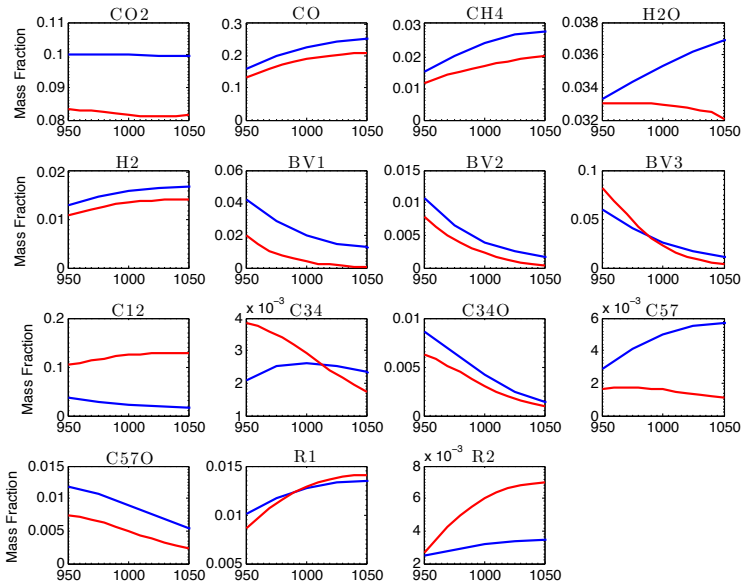

Figure 3.7: Equilibrium species mass fraction as a function of PaSR temperature: Comparison between detailed model prediction (blue line) and global model predictions (red lines).

CHAPTER 4

REACTIVE PSEUDO-2D BUBBLING FLUIDIZED BED SIMULATION USING A GLOBAL MODEL

4.1 Numerical Approach

A pseudo-2D simulation of a reactive bubbling fluidized bed was carried out to study the impact of feed-injection on granular mixing and chemical processes. The Lagrangian particle tracking approach and its coupling with the LES/DNS flow solver NGAis described in Pepiot and Desjardins [14, 4]. Solid phase chemistry has been implemented by augmenting each biomass particle to carry the species mass fractions representing the particle composition. No intra-particle processes are accounted for: each particle is treated as a single, homogeneous, entity, which allows for an easy treatment of polydisperse mixtures of variable density solid particles. The lumped chemistry model proposed by Miller and Bellan is used here [12] . The mechanism includes three reactions for each solid phase constituent:

$$\text{virgin(s)} \rightarrow \text{active(s)} \qquad \text{R1},$$
$$\text{active(s)} \rightarrow \text{tar(g)} + \text{gas(g)} \qquad \text{R2},$$
$$\text{virgin(s)} \rightarrow \text{active(s)} \qquad \text{R3},$$

And one gas phase reaction:

$$\text{tar(g)} \rightarrow \text{gas(g)} \qquad \text{R4}.$$

The feedstock composition used at present is one of the compositions (Beech) used by Miller and Bellan for validation purposes during the development of

the mechanism [12].

4.2 Results

Results obtained for a 2″ fluidized bed reactor are reviewed here. The geometry and the running conditions for these simulation are shown in Fig. 4.1 and Table 4.1. Three cases were chosen to investigate how the injection strategy can

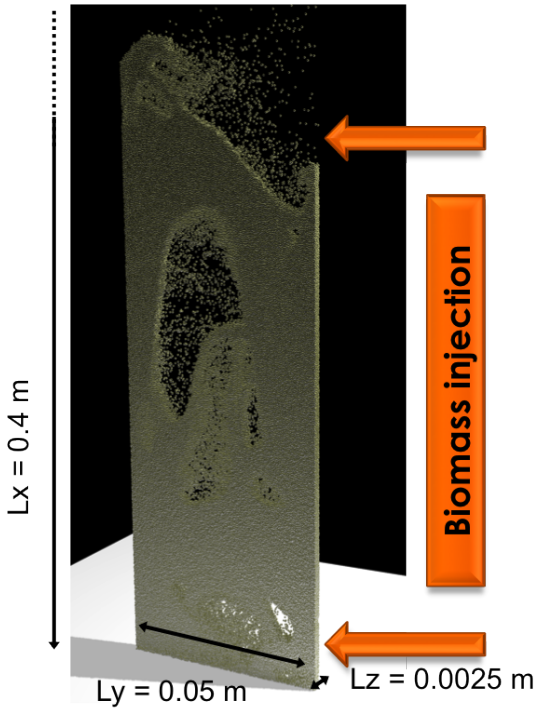

Figure 4.1: 2″ fluidized bed geometry, with the two injection cases illustrated.

affect biomass mixing and reaction rates: one cold case with just sand, a second case with injection of biomass at the bottom of the reactor, and a third case with injection of biomass at the top of the bed. Snapshots of the sand location at the start of biomass injection, and tar, gas and biomass location after a few ms are

shown in Figs. 4.2(a), 4.2(b), and 4.2(c). It appears that after a short time, the injected biomass particles are uniformly distributed in the bed. However, the most reactive particles will tend to congregate in a specific region of the dense bed, leading to locally high concentration in tar and gas.

To get a more quantitative perspective, statistics are gathered on the respective location of biomass and sand particles, now accounting for particle history (e.g. through the size of the biomass particles). In Fig. 4.3, the particle size segregation along the length of the reactor is shown. One can see that after about 3 seconds of simulation, the average particle diameter decreases slightly as we approach the top of the bed, verifying particle segregation, a phenomenon often observed in fluidized bed reactors. Another question of interest is how well the fluidized bed is achieving mixing of the biomass. The average biomass volume fraction along the reactor length for the top and bottom injection cases are compared at early and later times in Figs. 4.4 and 4.5. One can see in Fig. 4.4 that initially the biomass is concentrated in the region of injection. But after only a few seconds of simulation (Fig. 4.5), there is a fairly uniform biomass volume fraction along the bed in both the bottom and top injection cases, indicating that both strategies for injection are achieving good mixing.

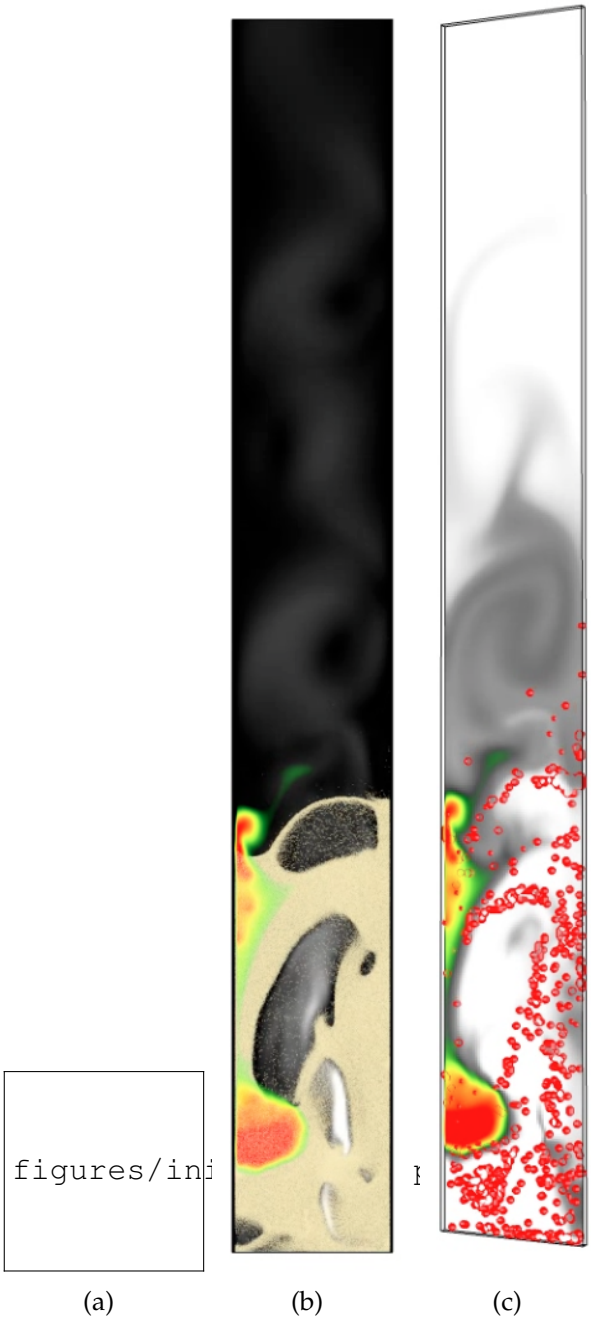

Figure 4.2: Snapshots from 2″ fluidized bed reactor simulation: a) Initial sand particles distribution b) Sand and tar levels shortly after injection c) Biomass distribution shortly after injection

Table 4.1: Wood particle geometric parameters

Parameter	Value (μm)
Gas and Sand Temperature	973K
Number of Particles	460, 000
Gas Inlet	Pure Nitrogen
Gas inlet Velocity	.292 m/s ($3U_{mf}$)
Biomass Injection mass flow rate	1E-05 kg/s
Biomass injection Temperature	300 K

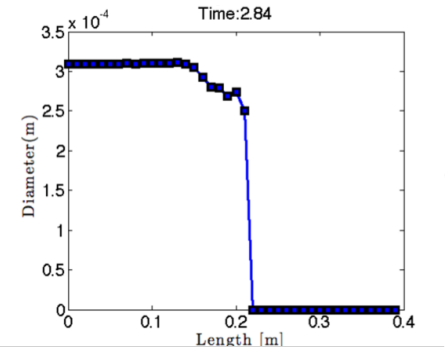

Figure 4.3: The average particle diameter across the length of the reactor.

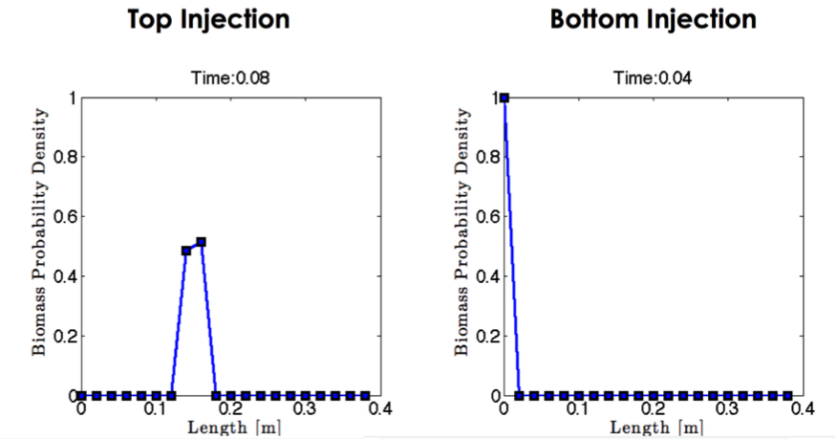

Figure 4.4: The initial biomass volume fraction along the length of the reactor for the top (left) and bottom (right) injection cases. Initially the biomass is concentrated in the respective injection regions.

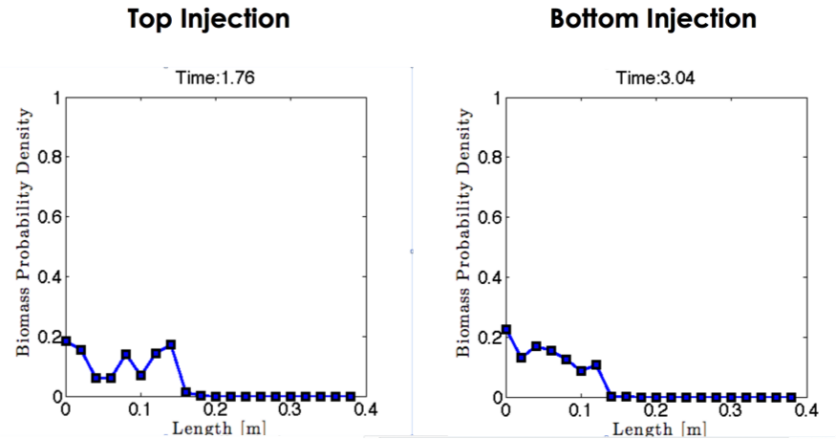

Figure 4.5: The biomass volume fraction along the reactor length for the top (left) and bottom (right) injection cases. Both cases appear to be achieving good mixing of the biomass after a short simulation time

APPENDIX A

CHARACTERIZATION AND MODELING OF WOOD MICROSTRUCTURE AND CHEMICAL COMPOSITION DURING CONVERSION.

A.1 Development of model geometry for wood microstructure

A.1.1 Introduction

There has recently been an interest in using modeling to study the thermo-chemical degradation of biomass on the intra-particle scale. The microstructure as well as the chemical make up of wood is complex, and therefore with a more fundamental understanding of their interaction, heating conditions and/or chemical catalysts can be chosen to improve the overall product yields. Previously in the literature, there have been a number of attempts to model thermo-chemical degradation at the particle scale: the most complex systems incorporate many coupled phenomena including heat transfer by convection and diffusion, chemical reaction kinetics, convection and diffusion of gaseous species through the porous material (defined by Darcys Law), and an internal build up of pressure as the reaction generates gas. However, these models lack a realistic representation of the biomass particle microstructure. Experimental measurements have shown that wood can have a void volume fraction as high as seventy-two percent [11]. It is clear that the microstructure will play a significant role in the heat and transport properties of the particle. Therefore, a method has been developed to generate a model geometry based on experimentally-measured geometric parameters. With this tool, a realistic geometry can be

generated for any biomass feedstock with known micro-structural properties and utilized in thermo-fluid simulations to give a more realistic depiction of the wood degradation process.

A.1.2 Method and results

A mathematical technique was developed to generate a realistic particle geometry based on a set of experimentally measured parameters. The major geometric characteristics of a wood considered in this method are depicted in Fig. A.1.2. The major components include: lumen, which are long cylindrical void spaces, cell wall, made up of mixture of complex polymers separating lumen, and pits, which are small holes in the cell wall connecting adjacent lumen. For example, experimentally measured parameters for Spruce wood, a feedstock commonly used in thermochemical conversion, were gathered from the literature in Table A.1.2.

The developed method will utilize these geometric parameters to generate a physically realistic model geometry for simulation as follows. Given a user defined volume space, a three dimensional grid of nodes is initialized as solid cell wall. Then, a possible set of lumen tangential and radial diameters is generated that represent a normal distribution based on the measured mean and standard deviation values. The algorithm finds the maximum number of lumen in two dimensions that can fit in the specified volume space. Similarly, the lumen lengths are normally distributed and start at random points in the z axis. Any node found on or within a lumen is defined as void space. Lastly, pits are randomly distributed in the cell wall structure in order to fit the measured pit

density (again setting those nodes to void space).

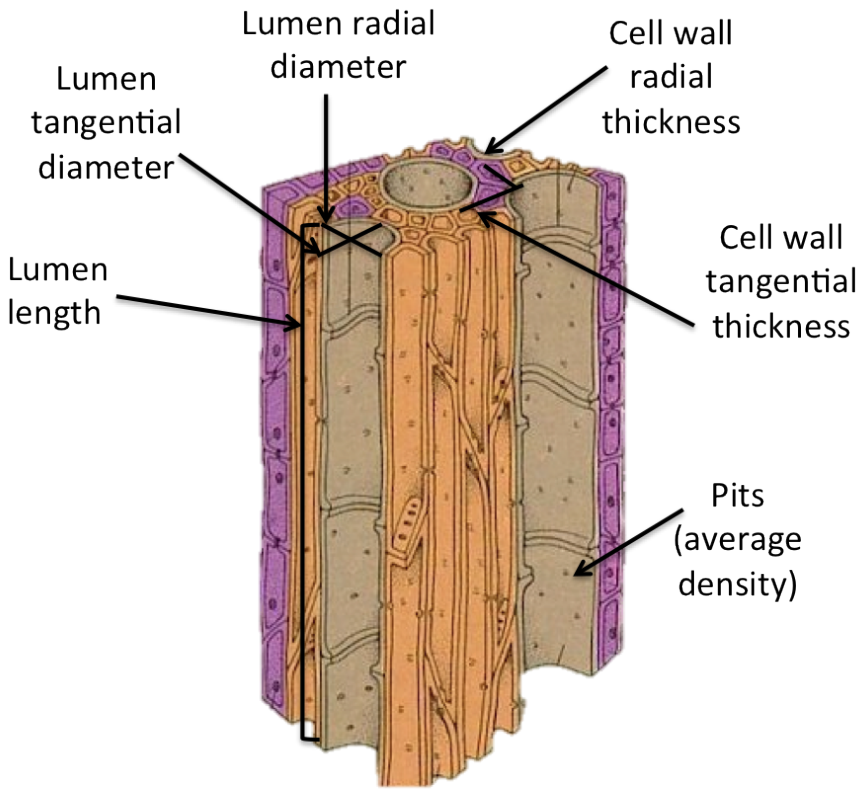

Figure A.1: Evolution of species mass fractions in a PaSR reactor model for biomass gasification: Comparison between detailed model prediction (blue line) and global model predictions (red lines).

A volume of specified size .1 mm x .1 mm .1 mm was generated to fit the geometric properties of spruce wood, the volume rendering of the geometry is shown in Fig A.1.2 One should note that the Matlab method described was developed in a flexible way, so that it may be used to produce accurate physical models for any wood strain with defined geometric properties. The geometry shown above has been utlized in some preliminary computational thermo-fluid simulation of wood degradation. The method as well as the results of the simulation are documented in Grout *et al* [9], with the expectation that the generated

Table A.1: Wood particle geometric parameters

Parameter	Value (μm)	Source
Lumen tangential diameter	35.3 ± 5.9	[21]
Lumen radial diameter	35.0 ± 6.4	[21]
Lumen length	2500 - 5000	[21]
Cell wall tangential thickness	2.99 ± 0.58	[21]
Cell wall radial thickness	3.16 ± 0.70	[21]
Pit Density	77 ± 35	[19]

geometry will be utilized in more comprehensive thermo-chemical simulations in the near future [1] .

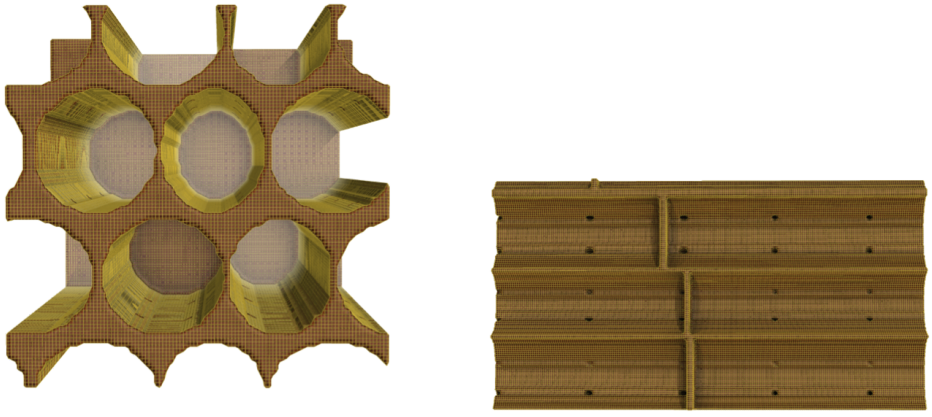

Figure A.2: Wood particle geometry

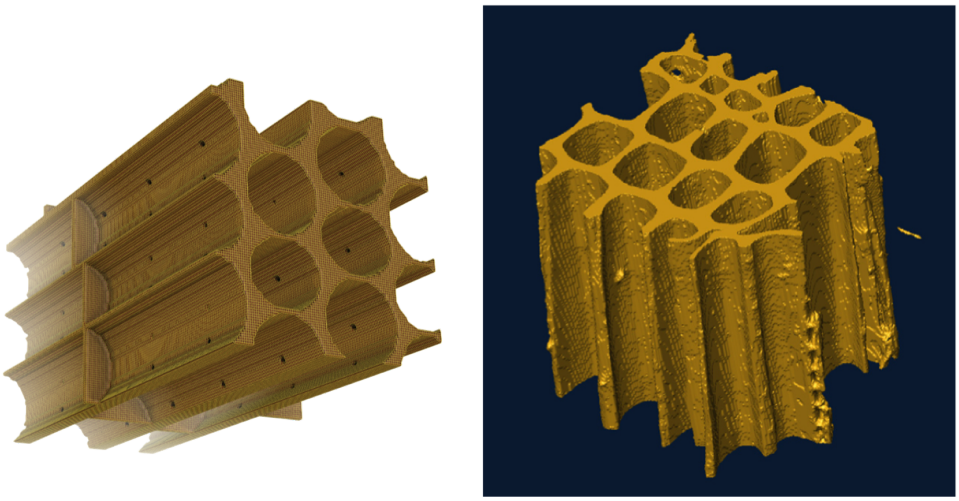

Figure A.3: Comparison of model geometry (left) to TEM images (right) from Trtik *et al* [21]

A.2 Chemical characterization of wood by Raman Spectroscopy

Methods have been developed to utilize Raman spectroscopy as a tool to chemically characterize wood structure. While techniques already exist to quantify the chemical composition of wood, Raman spectroscopy provides advantages to the established techniques. In addition to Raman spectroscopy being a non-invasive and quick method for chemical characterization, it provides the possibility of visualizing chemical composition in the context of the biomass structure. In recent studies, the prominent peaks in Raman spectra taken from poplar wood have been identified. Shown below is a Raman spectrum taken of a poplar wood section with NREL's 785 nm laser; the strongest signal peaks are labelled as identified by Gierlinger *et al* [8].

Raman spectroscopy can also be used to create hyperspectral maps, which

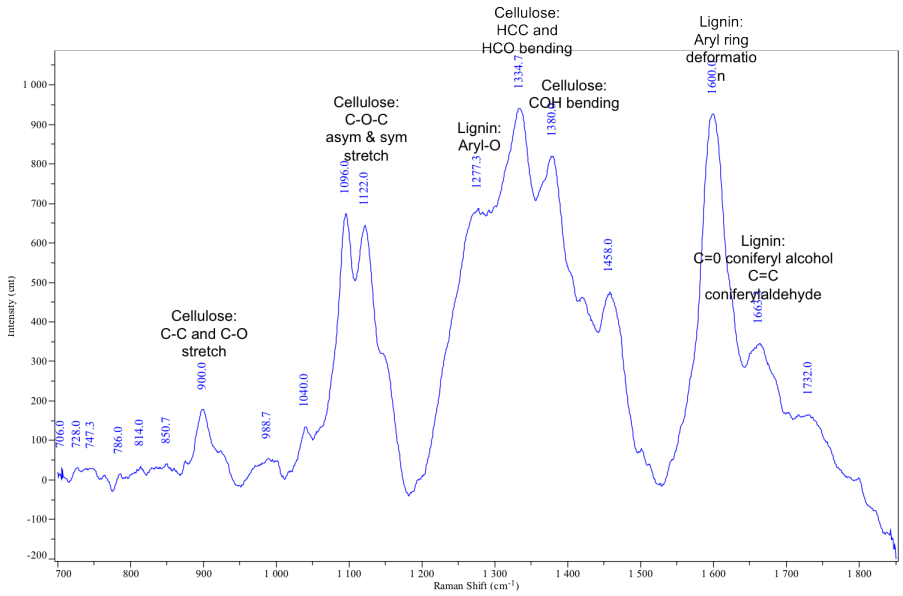

Figure A.4: Raman spectrum obtained with NREL's 785 nm laser

will be most useful in correlating wood structure and composition. To create a hyper spectral map, a set of Raman scans are taken across a grid of points as shown in Fig. A.5A. The goal of our work is to develop a methodology to convert this hyper spectral data into a chemical composition map. For example, to visualize the relative lignin content as a function of space in wood, the average signal intensity in the range 1550 to 1640 cm $^{-}$1 (a peak correlated to aryl ring deformation in lignin) is plotted at each grid point, as shown in Fig. A.5B. To extend this concept for more general compositional information the following methodology has been outlined. Raman spectra were taken of poplar wood samples of known varying composition (as determined by wet-lab techniques). Then we employ a linear algebraic approach to determine which peak intensities can be used to predict the composition. For example, Fig. **??**. shows Raman spectra for four poplar wood samples of varying lignin content, and the peaks associated with carbohydrates and lignin have been indicated in blue and red

respectively. Using the known composition of each sample and the relative peak intensities for each sample, the peaks that most significantly predict composition are identified. Then, with the correct mapping correlations one can predict composition of a sample of unknown characteristics. While this method needs to be developed further with a larger sample database, in order to display the abilities of the method, the mapping matrix obtained with four samples was used to map the composition of the Raman hyper spectra image as shown in Fig. A.2.

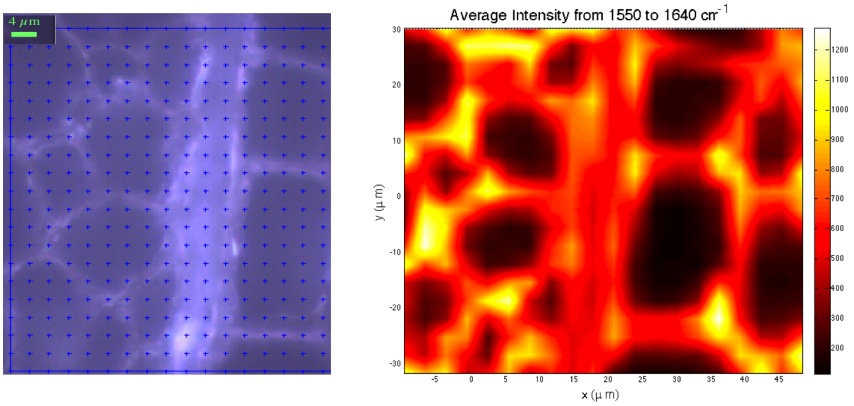

Figure A.5: A: grid of points at which a Raman scan was taken. B: hyper spectral map of lignin peak.

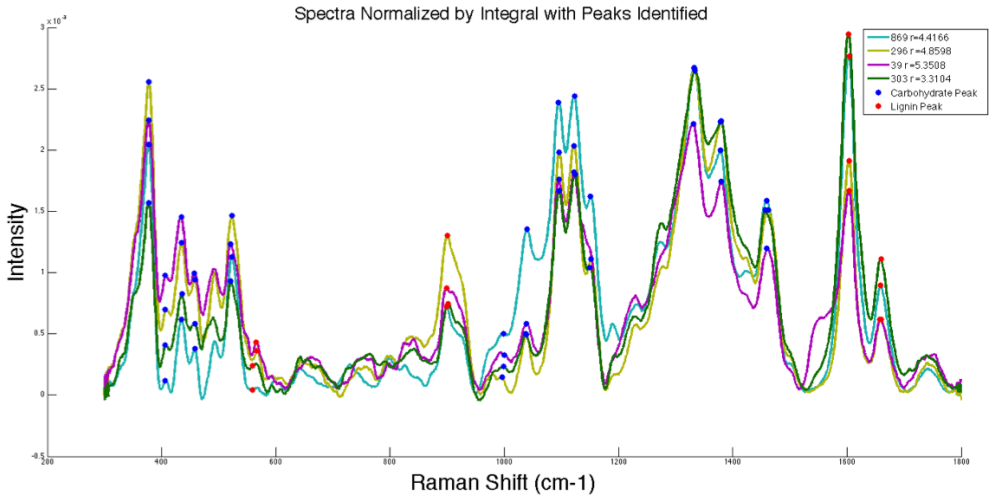

Figure A.6: Four samples with known varying lignin contents

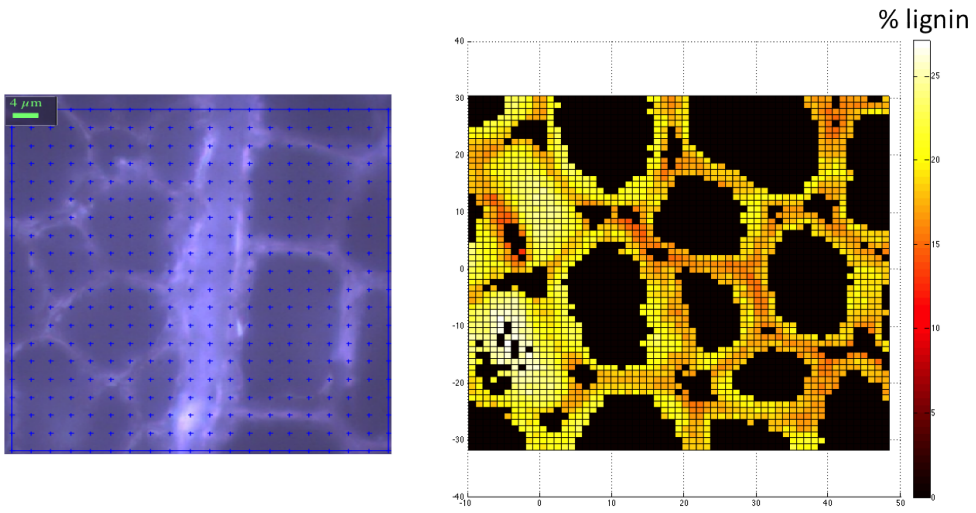

Figure A.7: Four samples with known varying lignin contents

APPENDIX B

INCORPORATION OF GLOBAL KINETICS INTO TECHNO-ECONOMIC ANALYSES

The developed global kinetic model for gasification has been transferred to a group at NREL conducting techno-economic analyses. The group focuses their studies in a software called Aspen. For the present, the focus of the group was on defining the chemical reactions and mixing that is occurring in the fluidized bed reactor unit. For this step, they have incorporated the global kinetic model developed above, and will be presenting their results in the future [20].

APPENDIX C

USE OF RAMAN SPECTROSCOPY TO ASSESS THE DEACTIVATION OF ZSM-5 CATALYST DURING VAPOR PHASE UPGRADING

There is a recent interest in fast pyrolysis for the high production of bio-oils. However, the bio-oils tend to be acidic and unstable, therefore an additional step known as catalytic vapor phase upgrading has shown promise in transforming the bio-oils into a product that can directly be incorporated as a drop in fuel. There are a few catalysts which have preformed particularly well in vapor phase upgrading, one of which is a ZSM-5 catalyst. In order to better define how the catalyst should be utilized in the pyrolysis process, it is necessary to characterize its deactivation properties. In this study, Raman spectroscopy was used to analyze five samples of UPV2 at different stages of deactivation. It was found that Raman spectroscopy is both an efficient and reliable tool to characterize the said catalyst. These findings have been incorporated into a broader study on vapor phase upgrading. [13]

BIBLIOGRAPHY

[1] P. Ciesielski, K. Malhotra, B. Donohoe, and M. Nimlos. Construction of Biomass Particle Models From Microscopy Data for Simulation of Transport Phenomena With Realistic System Geometry. *AICHE Conference (submitted)*, 2013.

[2] A Cuoci, T Faravelli, and A Frassoldati. *A General Mathematical Model of Biomass Devolatilization Note 1. Lumped kinetic models of cellulose, hemicellulose and lignin.*, 2007.

[3] A Cuoci, T Faravelli, and A Frassoldati. *A General Mathematical Model of Biomass Devolatilization Note 2.Detailed kinetics of volatile species.*, 2007.

[4] O. Desjardins, G. Blanquart, G. Balarac, and H. Pitsch. High order conservative finite difference scheme for variable density low Mach number turbulent flows. *J. Comp. Phys.*, 227(15):7125–7159, 2008.

[5] C. Di Blasi. Modeling chemical and physical processes of wood and biomass pyrolysis. *Prog. Energy. Combust. Sci.*, 34:47–90, 2008.

[6] T. Faravelli, A. Frassoldati, G. Migliavacca, and E. Ranzi. Detailed kinetic modeling of the thermal degradation of lignins. *Biomass and Bioenergy*, 34:290–301, 2010.

[7] K. R. Gaston, M. W. Jarvis, K. M. Smith, P. Pepiot, W. J. Frederick, and M. R. Nimlos. Biomass pyrolysis and gasification of varying particle sizes in a fluidized bed reactor. *Energy and Fuel*, 25:3747–3757, 2011.

[8] N. Gierlinger and M. Schwanninger. Chemical imaging of poplar wood cell walls by confocal Raman microscopy. *PlantPhys*, 140:1246, 2006.

[9] R. Grout, K. Malhotra, P. Ciesielski, K. Gruchalla, B. Donohoe, and Nimlos. Computational assessment of the effect of realistic intraparticle geometry on biomass heating rates and pyrolysis yields. *Proceedings of 2010 Spring Meeting of the Western State Section of The Combustion Institute, Boulder, CO*, 2013.

[10] M. W. Jarvis, T. J. Haas, B. S. Donohoe, J. W. Daily, K. R. Gaston, W. J. Frederick, and M. R. Nimlos. Elucidation of biomass pyrolysis products using a laminar entrained flow reactor and char particle imaging. *Energy and Fuel*, 25:324–336, 2011.

[11] S.C. Mayo, F. Chen, and R. Evans. Micron-scale 3D imaging of wood and plant microstructure using high-resolution X-ray phase-contrast microtomography . *J. Str. Bio.*, 171:182–188, 2010.

[12] R. S. Miller and J. Bellan. A generalized biomass pyrolysis model based on superimposed cellulose, hemicellulose and lignin kinetics. *Combust. Sci. Tech.*, 126:97–137, 1997.

[13] C. Mukarakate, X. Zhang, D. Robichaud, P. Ciesielski, K. Malhotra, B. Donohoe, K. Iisa, and M. Nimlos. Online monitoring of upgraded vapors during catalytic fast pyrolysis of pine: Effect of ZSM-5 catalyst deactivation. *TC Biomass (submitted)*, 2013.

[14] P. Pepiot and O. Desjardins. Numerical analysis of the dynamics of two- and three-dimensional fluidized bed reactors using an Euler-Lagrange approach. *Powder Tech.*, 2011, in press.

[15] P. Pepiot, M. W. Jarvis, M. R. Nimlos, and G. Blanquart. Proceedings of 2010 spring meeting of the western state section of the combustion institute, boulder, co, 2010.

[16] N. Prakash and T. Karunanithi. Kinetic modeling in biomass pyrolysis -a review. *J. App Sci Res.*, 12:1627–1636, 2008.

[17] R. Radmanesh, Y. Courbariaux, J Chaouki, and C. Guy. A unified lumped approach in kinetic modeling of biomass pyrolysis. *Fuel*, 85(9):1211–1220, June 2006.

[18] E. Ranzi, A. Cuoci, T. Faravelli, A. Frassoldati, G. Migliavacca, S. Pierucci, and S. Sommariva. Chemical kinetics of biomass pyrolysis. *Energy and Fuel*, 22:4292–4300, 2008.

[19] Y. Sano, H. Morris, H. Shimada, L. Ronse De Craene, and S. Jansen. Anatomical features associated with water transport in imperforate tracheary elements of vessel-bearing angiosperms. *AnnalsBotany*, 107:953–964, 2011.

[20] A. Trendewicz, A. Dutta, S. Czernik, K. Malhotra, Pepiot P., and R. Braun. Fluidized Reactor Model For Biomass Fast Pyrolysis. *TC Biomass (submitted)*, 2013.

[21] P. Trtik, J. Dual, Keunecke D., D. Mannes, P. Niemz, P. Stahli, A. Groso, and

M. Stampanoni. 3D imaging of microstructure of spruce wood. *J. Str. Bio.*, 159:46–55, 2007.

[22] Y. Wang and C.M Knishita. Kinetic model of biomass gasification. *Solar Ener.*, 51:19–25, 1993.